

RaindropGS: A Benchmark for 3D Gaussian Splatting under Raindrop Conditions

Zhiqiang Teng¹ Tingting Chen² Beibei Lin² Zifeng Yuan²

Xuanyi Li¹ Xuanyu Zhang¹ Shunli Zhang¹

¹Beijing Jiaotong University, ²National University of Singapore

24115171@bjtu.edu.cn, tinting.c@u.nus.edu beibei.lin@u.nus.edu, zyuan@u.nus.edu

24110477@bjtu.edu.cn, 24115169@bjtu.edu.cn, slzhang@bjtu.edu.cn

Abstract

*3D Gaussian Splatting (3DGS) under raindrop conditions suffers from severe occlusions and optical distortions caused by raindrop contamination on the camera lens, substantially degrading reconstruction quality. Existing benchmarks mainly rely on synthetic raindrop datasets with known camera poses (constrained images), assuming ideal conditions. However, in real-world scenarios, raindrops severely hinder accurate pose estimation and point cloud initialization, while the large domain gap between synthetic and real data further limits generalization. To tackle these issues, we introduce **RaindropGS**, a comprehensive benchmark designed to evaluate the full 3DGS pipeline—from unconstrained, raindrop-corrupted images to clear 3DGS reconstructions. We first collect real-world paired 3D scenes, each containing three aligned image sets: raindrop-focused, background-focused, and rain-free ground truth. These real-world data enable reliable evaluation of reconstruction quality under different focus conditions. Building on this foundation, our benchmark estimates camera poses and initializes point clouds from raindrop-corrupted images, followed by raindrop removal for 3D Gaussian optimization. This setup enables end-to-end evaluation of how errors accumulated across the 3DGS reconstruction pipeline affect the final reconstruction quality under real-world raindrop interference. Through comprehensive experiments and analyses, we reveal critical insights into the performance limitations of existing 3DGS methods on unconstrained raindrop images and quantify the impact of individual pipeline components. These insights establish clear directions for developing more robust 3DGS methods under raindrop conditions.*

1. Introduction

3D Gaussian Splatting (3DGS) in raindrop-contaminated scenes presents significant challenges [4, 16, 25], as adherent raindrops on camera lenses cause severe occlusions and optical distortions [3, 17, 18, 27, 41]. These artifacts disrupt image correspondence, degrade the quality of camera pose estimation and point cloud initialization [13, 21, 36, 44], both of which are essential for successful 3DGS reconstruction. Moreover, the presence of raindrops varies across views, blurring images by changing the camera focal plane [15, 16, 39, 39, 40], introducing multi-view inconsistencies that further hinder reconstruction fidelity [19, 26].

Several recent methods [17, 18, 27] have explored 3D Gaussian Splatting under raindrop scenarios and demonstrated promising results on synthetic datasets. However, such evaluation settings are overly idealized and fail to capture the complexity and diversity of real-world conditions. To be specific, these methods typically assume the raindrop inputs are constrained images, where a clear details of both raindrops shape and background scenes, a good camera pose and point cloud initialization. However, acquiring such information from real-world raindrop-affected images is challenging [9, 23, 43]. Inaccuracies in pose estimation and point cloud initialization can significantly degrade the quality of subsequent 3DGS reconstruction [5, 9, 34]. Furthermore, the substantial domain gap between synthetic and real raindrops raises concerns about generalization. Methods validated on synthetic datasets often fail to perform well when applied to real-world scenes.

To address these issues, we introduce **RaindropGS**, a comprehensive benchmark for evaluating the complete raindrop 3DGS pipeline—from unconstrained, raindrop-corrupted input images to clear 3DGS reconstructions. As illustrated in Figure 1, our pipeline consists of three stages: data preparation, data processing, and raindrop-aware 3DGS evaluation. For data preparation, we compare

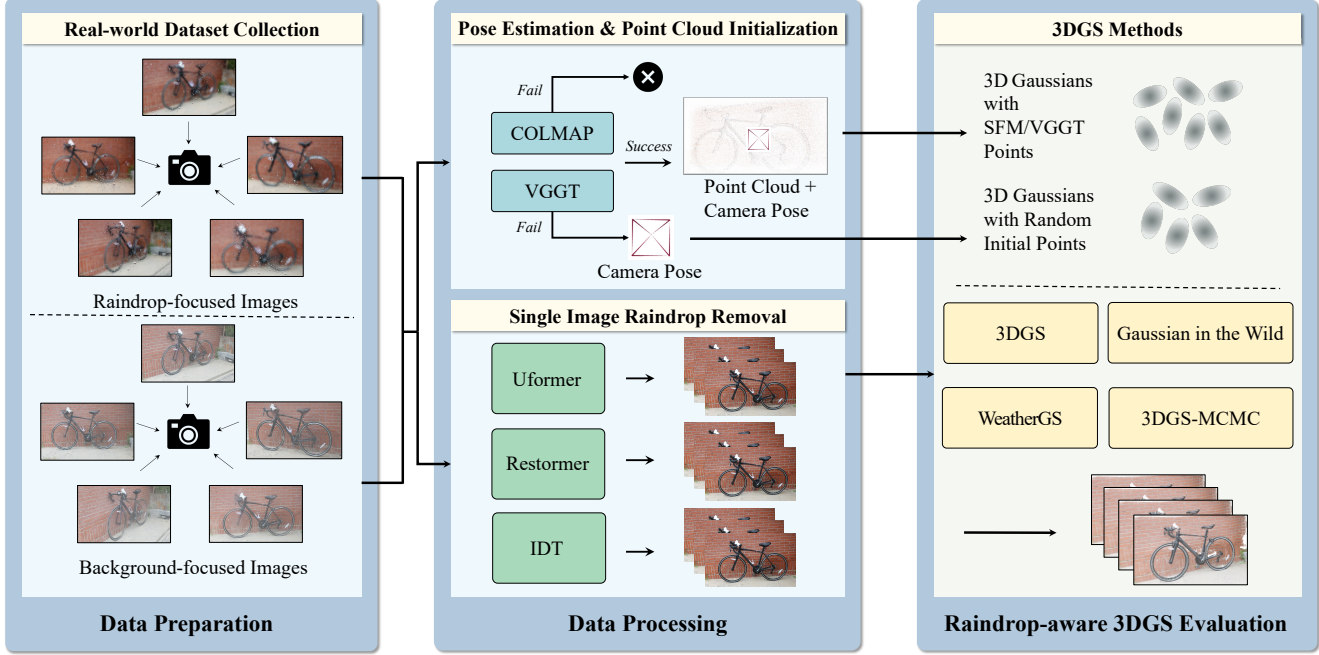


Figure 1. 3DGS Raindrop Reconstruction Benchmark Pipeline. We develop the first benchmark for comprehensively evaluating 3DGS performance under raindrop conditions. The benchmark begins with real-world dataset collection, proceeds through data processing, and ends with a raindrop-aware 3DGS evaluation. In particular, we assess how raindrop-induced image contamination reduces the number of points available for cloud initialization and degrades camera pose estimation, and how these factors impact the performance of 3DGS methods.

the effects of different types of images (raindrop-focused and background-focused) on the subsequent reconstruction process. During data processing, we evaluate the performance of camera pose estimation and point cloud initialization, as well as single-image raindrop removal algorithms. In raindrop-aware 3DGS evaluation, we consider methods that may affect the performance of real-world raindrop reconstruction, such as raindrops and point cloud Gaussian optimization.

As illustrated in Figure 2 (a-c), these synthetic datasets are valuable but exhibit limitations, such as the same raindrop shape and position across different views. To overcome these limitations, we collect a real-world 3D reconstruction dataset captured under raindrop conditions. For each scene, three aligned image sets are acquired: raindrop-focused, background-focused, and rain-free ground truth. This design enables evaluation of the full pipeline in real-world scenarios as well as under different focus conditions. As shown in Figure 2 (d), our RaindropGS dataset reflects real-world conditions, featuring multiple focus settings and a diverse range of raindrop characteristics.

Using the collected dataset, we process the images (both raindrop-focused and background-focused) to obtain the corresponding rain-free images, estimated camera pose, and initialized point cloud. To analyze the impact of raindrops on the real-world dataset collection, we use

COLMAP [31] and VGGT [35] to estimate the camera pose and initialize the point cloud, enabling us to investigate how sequence-based and feed-forward approaches influence the performance of 3DGS methods. We include three widely used deraining methods, Uformer [37], AtGAN [28], Restormer [42], and IDT [38] in the raindrop removal stage, comparing the impact of different raindrop removal methods on subsequent 3DGS reconstruction performance. For the raindrop-aware 3DGS evaluation, we integrate multiple 3DGS variants, including the original 3DGS [11], WeatherGS [27], GS-W [43], and 3DGS-MCMC [12], to evaluate the impact of different reconstruction strategies on raindrop-corrupted inputs. These methods are evaluated under varying pre-processing pipelines and focus conditions to assess their robustness and adaptability.

Through rigorous quantitative and qualitative analyses, we evaluate the performance of state-of-the-art 3DGS methods under raindrop conditions, as well as their pre-processing stages. The results revealing their strengths, limitations, and sensitivity to different pre-processing and focus settings. These findings not only benchmark the current progress but also highlight key challenges and future directions for improving 3DGS performance in real-world adverse environments. Our main contributions are summarized as follows:

- We introduce the first 3DGS benchmark for raindrop

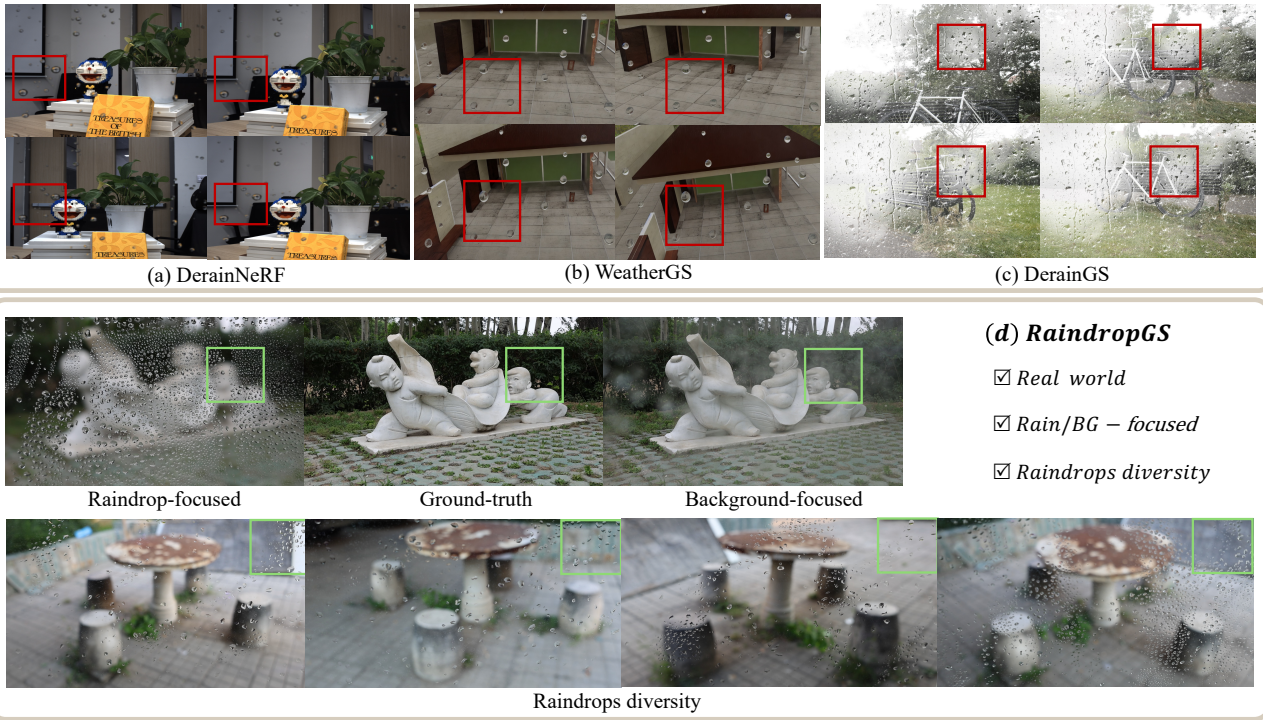


Figure 2. Example of existing raindrop 3D datasets (DerainNeRF [17], WeatherGS [27], DerainGS [18]) and our RaindropGS Dataset. As indicated by the red boxes, existing datasets exhibit the same raindrop distribution across different viewpoints; in contrast, the green boxes illustrate the diversity of raindrop distributions in our dataset. For each viewpoint, we include both raindrop-focused and background-focused images and provide corresponding clear images for 3DGS performance evaluation.

contaminated scenes, covering the complete pipeline from unconstrained, raindrop-corrupted images to the final 3D Gaussian reconstructions.

- We collect real-world paired 3D scenes, each containing three aligned image sets: raindrop-focused, background-focused, and rain-free ground truth, enabling comprehensive evaluation of reconstruction quality across different focus conditions.
- We comprehensively validate existing 3DGS methods on our benchmark, revealing their strengths and limitations, and providing insights into future research directions.

2. Related Work

3DGS Reconstruction under Raindrop Conditions In recent years, 3DGS has emerged as a powerful technique for scene reconstruction. Unlike NeRF [20], it represents scenes using a sparse set of 3D Gaussians, enabling real-time rendering [1]. However, standard 3DGS benchmarks assume clear input views, and performance often degrades when images contain transient occlusions such as raindrops on the lens [14, 18, 27].

To address this issue, several methods [17, 18, 27] have been developed to improve 3D reconstruction in raindrop scenes. WeatherGS [27] first generates raindrop masks to

identify occluded regions and then reconstructs clear scenes by excluding these areas during 3D Gaussian Splatting. Meanwhile, DerainGS [18] incorporates a dedicated image enhancement module to remove raindrop artifacts and employs supervised Gaussian-ellipsoid fitting, achieving 3D deraining in the final output. These methods are trained on synthetic raindrops and deliver strong results under the assumption of accurate camera pose estimation and reliable point cloud initialization. However, they overlook the initial disruptions that real raindrops introduce to both pose estimation and point cloud initialization, resulting in poor generalization to real-world raindrop scenarios.

Raindrop Removal Methods To mitigate lens occlusion artifacts, single-image derain methods have been extensively studied. Early works such as Raindrop Removal Network [29] leverage visual attention to segment and inpaint raindrop regions, while UMAN [32] extends this idea with multiscale feature fusion. AtGAN [28] removes raindrops using an attention-guided generative adversarial network that identifies raindrop regions and reconstructs the missing background. More recently, transformer-based restoration models (for example, Restormer [42], Uformer [37], DiT [24] and IDT [38]) demonstrate superior restoration

under heavy rainfall by modeling long range dependencies. However, these methods process each image independently and do not enforce cross-view consistency, leading to reconstruction artifacts when applied as a preprocessing step for 3D reconstruction.

3D Raindrop Reconstruction Benchmark and Dataset

Current 3DGS raindrop reconstruction methods focus primarily on the Gaussian fitting stage and ignore the influence of earlier steps on the training process, such as camera pose estimation and point cloud initialization. In addition, they rely on synthetic training datasets created by Blender on clear images [17, 18], which creates a significant domain gap and prevents accurate evaluation in real-world conditions. A few real-world datasets have tried to simulate rain on camera lenses for stereo or small scale multi view setups. DerainNeRF [17] captures stereo pairs by spraying water onto a glass plate in front of a calibrated rig and provides binary raindrop masks. WeatherGS [27] extracts key frames from publicly available rainy videos but does not supply a ground truth reference. Overall, existing datasets remain mostly synthetic and do not reflect real-world raindrop interference, and current algorithms overlook the early stages of the pipeline, making their performance evaluation under real conditions unreliable.

To address this challenge, we revisit the complete 3DGS raindrop reconstruction pipeline and develop a benchmark covering every stage: data preparation, data processing, and raindrop-aware 3DGS evaluation. To evaluate current algorithms and guide future research, we compile a real-world dataset of eleven scenes.

3. RaindropGS Benchmark and Dataset

Figure 1 illustrates the overall pipeline of our benchmark RaindropGS, showing the process from unconstrained raindrop-corrupted images to clean 3D Gaussian representations. It consists of data preparation, data processing, and raindrop-aware 3DGS evaluation.

Unlike existing methods that rely on synthetic datasets for quantitative evaluation, we collect real-world raindrop/ground-truth image pairs, enabling realistic assessment of each stage in the 3DGS reconstruction pipeline. Our data processing employs structure-from-motion (SfM) or feed-forward methods to estimate camera poses and initialize the point cloud. The raindrop-aware 3DGS evaluation measures the robustness of existing 3DGS methods under real-world challenges, including inaccurate point cloud initialization and imperfect raindrop removal.

3.1. Data Preparation

We first describe our data collection process, including the underlying optical refraction model and acquisition setup.

Table 1. Comparative raindrop 3D Reconstruction datasets. Compared to existing collections, our dataset spans a greater variety of scenes and distinguishes between raindrop-focused and background-focused captures.

Dataset	Scene count		Images (Real)	GT (Real)	Camera focus	
	Real	Synthetic			Raindrop	Background
DerainNeRF	3	2	20–25	×	×	✓
DerainGS	7	6	22–35	×	×	✓
RaindropGS	11	×	24–53	✓	✓	✓

We also present dataset statistics and comparisons with existing datasets.

Data Collection To begin with, we consider a pinhole camera model focused on the background plane [8]. In the absence of optical distortion (e.g., caused by raindrops), all scene elements located on the focal plane would appear sharp and well-defined [7]. However, raindrops adhering to a thin cover glass placed directly in front of the lens act as miniature convex lenses, introducing optical distortion and causing defocus [10]. When background rays intersect a raindrop, they are refracted at the curved surface of the drop decided by Snell Law [2]. In contrast, rays that do not encounter any raindrop travel without deviation through the imaging system to the sensor. Consequently, refracted and non-refracted rays map to spatially distinct locations on the image plane, illustrating how the presence of raindrops directly affects the imaging distortion. Furthermore, since raindrops don’t fully transmit light, the regions under raindrops exhibit localized intensity attenuation. This attenuation produces visible artifacts.

By contrast, another alternative configuration in which the camera is set to focus on the raindrop plane rather than the background plane. In this configuration, the image plane captures sharp, in-focus representations of the raindrop surfaces. Under these circumstances, more distant background features, seen through each raindrop, appear as miniaturized projections and are blurred in areas outside the raindrops.

To create the dataset, we use a pan-tilt sphere platform to keep the camera stationary. We then follow a standardized protocol grounded in optical refraction principles to ensure consistent camera alignment while allowing raindrops to vary in location, shape and size. The setup consists of two professional tripods with ball heads, a calibrated pressure sprayer, and a glass plate with over 98 percent light transmittance.

Data Statistics We summarize our dataset in Table 1. The dataset includes 11 real-world scenes, each containing 24 to 53 images captured under unconstrained raindrop conditions. For every viewpoint, three aligned images are pro-

vided: a raindrop-focused image, a background-focused image, and a clean ground-truth image. The raindrops in each viewpoint vary randomly in shape, number, and size, closely replicating real-world conditions. In contrast, existing synthetic datasets for 3DGS lack representation of camera focus effects on raindrop images and do not include diverse raindrop appearances across multiple viewpoints.

Focus Shift During image capture (Figure 2(d)), raindrops adhering to the front glass shift the camera’s focal plane. When many raindrops lie within the depth of field, the camera focuses on them and the background becomes blurred. Conversely, if only a few raindrops fall within the focal region, the camera focuses on the background and the raindrops appear out of focus. Most synthetic datasets ignore focus variation and render both background and raindrops as sharply in focus, which may reduce 3DGS reconstruction accuracy on real images. The RaindropGS dataset explicitly addresses this issue by capturing each scene under both raindrop-focused and background-focused conditions to support more realistic 3DGS raindrop evaluation.

3.2. Data Processing

Our data processing pipeline consists of two main components: pose estimation and point cloud initialization, and single-image raindrop removal pre-processing. Unlike existing raindrop Gaussian splatting methods that assume known camera poses and accurate point clouds, our benchmark directly estimates both the camera poses and an initial point cloud from the raindrop-affected images. This approach enables us to evaluate the robustness of the subsequent 3DGS reconstruction against potential errors in pose estimation and inaccuracies in the initial point cloud. To obtain a clean 3DGS reconstruction in the raindrop-aware 3DGS evaluation stage, we apply raindrop removal techniques to the multi-view raindrop images.

Pose Estimation and Point Cloud Initialization To estimate the camera pose and initialize the point cloud from multi-view raindrop images, we employ COLMAP [31] and Visual Geometry Grounded Transformer (VGGT) [35].

COLMAP is a robust tool capable of performing both Structure-from-Motion (SfM) [30] and Multi-View Stereo (MVS) [6]. We leverage SfM to estimate intrinsic and extrinsic camera parameters and MVS to generate the initial point cloud. However, raindrop interference often impedes reliable feature matching across viewpoints. This results in significant errors in estimated camera parameters and a drastic reduction in initialized point cloud density. To overcome the limitations of SfM, we employ VGGT as a comparative baseline. VGGT, a feed-forward unified method for pose estimation and point cloud generation, is more robust to raindrop interference due to its use of DINO [22].

In raindrop-focused scenes, the background is often too blurred for reliable scene initialization, causing both COLMAP [31] and VGGT [35] to fail. In certain scenes, COLMAP may suffer a substantial reduction in the number of matchable camera poses due to degraded Correspondence Search [31] performance, which ultimately leads to reconstruction failure. To address cases where raindrop interference and blur reduce the initial point cloud produced by COLMAP and VGGT, we employ a random point-cloud initialization strategy. Specifically, 100,000 points are randomly initialized, matching the order of magnitude of point counts obtained from ground-truth scenes.

Raindrop Removal Since traditional 3DGS methods do not incorporate raindrop removal capabilities, we employ four widely used single-image restoration models. Uformer [37] applies non-overlapping window-based self-attention and a multi-scale restoration modulator, demonstrating superior capability in restoring details from raindrop-affected and blurry images. Restormer [42] leverages multi-Dconv head transposed attention and a gated-Dconv feed-forward network to restore high-quality images, while IDT [38] employs a dual Transformer with window- and spatial-based designs for rain streak and raindrop removal. AtGAN [28] removes raindrops using an attention-guided generative adversarial network that identifies raindrop regions and reconstructs the missing background.

All raindrop removal methods are trained on the Raindrop Clarity dataset [10] to acquire raindrop removal capabilities. Raindrop Clarity is a dataset containing both daytime and nighttime image pairs, though we only use the daytime data for training. Furthermore, Raindrop Clarity includes both background-focused and raindrop-focused image pairs, making it well-suited for our task.

3.3. Raindrop-aware 3DGS Evaluation

With the estimated camera poses and initialized point cloud, we proceed to evaluate four representative 3DGS methods: 3DGS [11], WeatherGS [27], GS-W [43], and 3DGS-MCMC [12]. Among these, 3DGS [11] serves as a standard baseline for 3D Gaussian splatting. WeatherGS [27] incorporates single-image raindrop removal, so we omit the explicit raindrop removal step in its data processing pipeline. GS-W [43] is specifically designed for challenging conditions and unconstrained image collections, making it more robust to inconsistent multi-view inputs. 3DGS-MCMC [12], on the other hand, does not rely on accurate point cloud initialization. Each of the aforementioned methods has its own advantages, making their evaluation in our benchmark both meaningful and insightful.

Table 2. The quantitative evaluation of baseline approaches on the RaindropGS dataset. GS-W achieves the best performance with VGGT. These 3DGS variants excel on background-focused dataset but show significantly lower performance on raindrop-focused dataset. We highlight the **best** and **second-best** results for each metric.

Focus	Metrics	3DGS			3DGS-MCMC			GS-W			WeatherGS
		Uformer	Restormer	IDT	Uformer	Restormer	IDT	Uformer	Restormer	IDT	x
RD-focused	PSNR↑	13.894	13.876	13.958	15.109	15.005	14.994	16.099	15.400	15.873	13.070
	SSIM↑	0.346	0.345	0.350	0.383	0.380	0.383	0.512	0.484	0.511	0.307
	LPIPS↓	0.657	0.653	0.658	0.654	0.649	0.659	0.808	0.828	0.798	0.658
BG-focused	PSNR↑	17.906	17.741	18.094	18.219	18.148	18.239	19.123	19.074	17.818	17.124
	SSIM↑	0.478	0.469	0.480	0.482	0.477	0.483	0.555	0.550	0.507	0.428
	LPIPS↓	0.459	0.455	0.438	0.486	0.482	0.478	0.483	0.479	0.526	0.436



Figure 3. Qualitative Comparison among 3DGS methods: On the raindrop-focused dataset, the original 3DGS loses structural integrity, while GS-W and 3DGS-MCMC retains scene completeness. WeatherGS faithfully reconstructs the scene after raindrop removal but fails to correct background blur. On the background-focused dataset, all methods show moderate performance with artifacts.

4. Experiments

4.1. Implementation Details

We standardize all scene images to a resolution of 1024 * 576 for uniform comparison. During VGGT-based camera pose estimation and point cloud initialization, we follow the preprocessing protocol of VGGT [35], resizing each input image to 518 * 518 before processing. Likewise, for Restormer [42] and IDT [38], we downscale images to 128 * 128; for Uformer [37] and AtGAN [28], we downscale images to 256 * 256, and then tile the results to restore the original resolution.

For all 3DGS methods, we follow the official optimization settings: 30,000 iterations for 3DGS, WeatherGS, and 3DGS-MCMC, and 70,000 iterations for GS-W.

For 3DGS-MCMC, we set the initial point cloud size to 100,000, based on the number of points that VGGT can initialize in our dataset. All models are implemented in PyTorch and trained on 8 NVIDIA RTX 3090 GPUs.

4.2. Quantitative Comparison

Table 2 compares the impact of background-focused (BG-focused) and raindrop-focused (RD-focused) captures on 3DGS performance using VGGT [35]. For the original 3DGS method, raindrop-focused images exhibit a 4 dB drop compared to background-focused images, due to background blur and light refraction. VGGT processes all scenes but generates a point cloud with 0 points for raindrop-focused images, for which we use a randomly initialized point cloud.

Table 5 and Table 4 compares the performance of VGGT [35] and COLMAP [31]. For camera pose estimation, we use VGGT and COLMAP to estimate poses on the ground-truth images and compare these estimates with the poses obtained from the corresponding images. VGGT yields more accurate camera pose estimates; both methods accurately recover poses for background-focused images but exhibit substantial performance degradation on raindrop-focused images. In terms of point cloud initialization, VGGT outperforms COLMAP for background point clouds, yet it fails to initialize the raindrop-focused dataset.

Table 3. Comparison of the performance of different raindrop removal and restoration methods. BG-focused = background-focused, RD-focused = raindrop-focused. All model weights are taken from Raindrop Clarity and evaluated under the officially recommended settings. We highlight the **best** and **second-best** results for both background-focused and raindrop-focused datasets.

Metric	AtGAN		IDT		Restormer		Uformer	
	BG-focused	RD-focused	BG-focused	RD-focused	BG-focused	RD-focused	BG-focused	RD-focused
PSNR \uparrow	22.366	19.758	24.203	19.847	28.442	24.055	28.997	24.465
SSIM \uparrow	0.683	0.458	0.765	0.481	0.861	0.708	0.880	0.736
LPIPS \downarrow	0.233	0.365	0.157	0.344	0.108	0.235	0.106	0.218

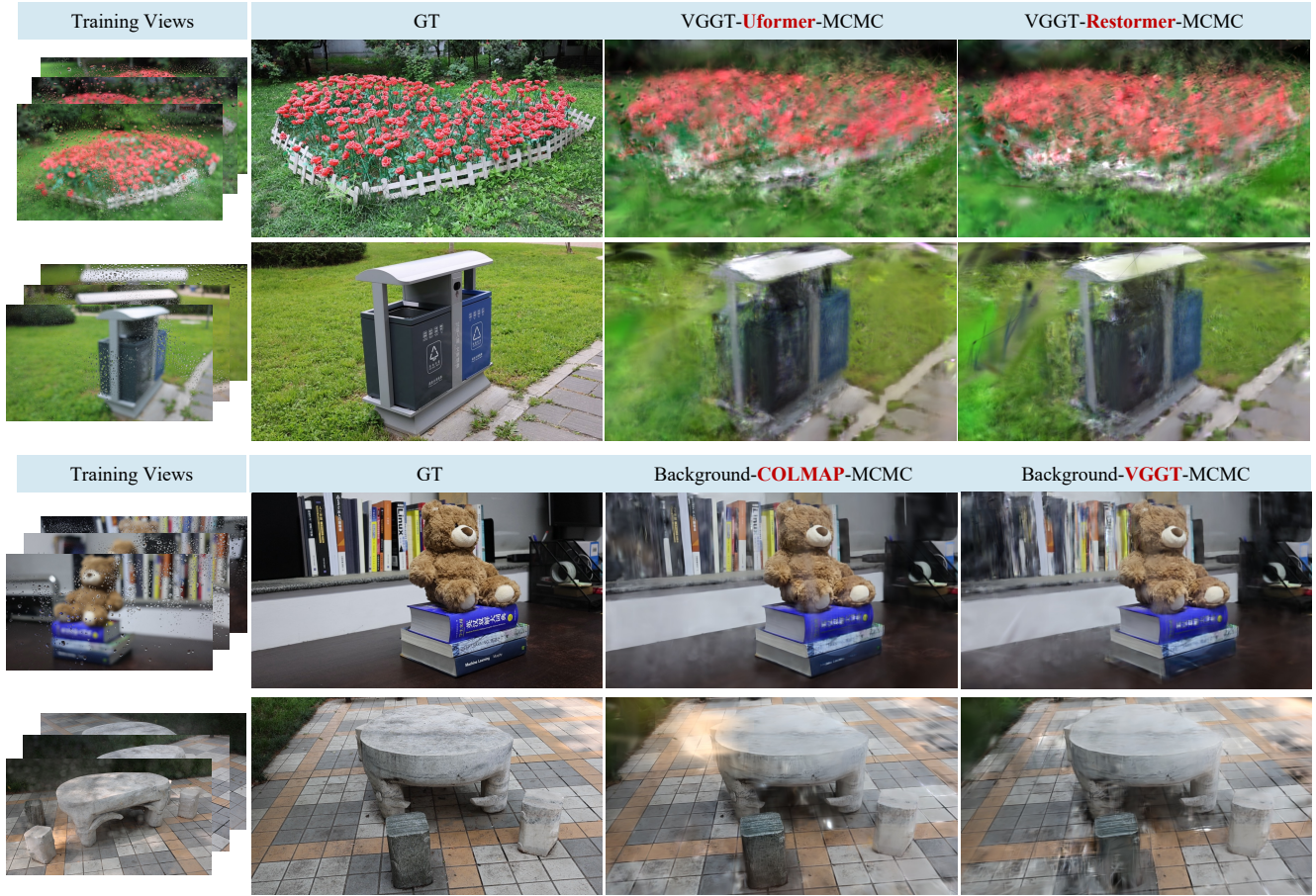


Figure 4. Qualitative Comparison across data pre-processing: Uformer and Restormer exhibit comparable raindrop removal capability. While COLMAP, when successful in estimating camera poses, reconstructs more fine-grained details than VGGT.

Table 3 reports the performance of different deraining and restoration methods on raindrop-affected images. Uformer [37] and Restormer [42] show comparable results, with Uformer [37] slightly outperforming Restormer [42] in reconstruction metrics, while IDT [38] lags substantially behind the other two methods.

For 3DGS methods, GS-W [43] with VGGT [35] and Uformer [37] preprocessing achieves the best performance (PSNR = 19.123), due to its adaptive optimization strategy for handling occlusions and environmental variations in outdoor scenes. The second best is 3DGS-MCMC [12] (PSNR

= 18.239) on background-focused scenes with IDT [38] and VGGT, which shows robustness to initialization.

4.3. Qualitative Comparison

Figures 3 and 4 show the qualitative results of 3DGS [11], WeatherGS [27], GS-W [43], and 3DGS-MCMC [12], along with their Uformer [37] and Restormer [42] outputs. Scenes with background-focused images exhibit generally good performance, while raindrop-focused images pose significant reconstruction challenges due to the loss of background details and the presence of undetected rain-

Table 4. Quantitative analysis of the impact of camera pose estimation and point cloud initialization using COLMAP [31] and VGGT [35] on 3DGS raindrop reconstruction performance. Three reconstruction methods, 3DGS [11], GS-W [43], and WeatherGS [27], are used for testing. COLMAP failed entirely on the raindrop-focused dataset; only background-focused results are reported. “ \times ” indicates reconstruction failures caused by unsuccessful camera pose estimation. We highlight the best and second-best results for each scene.

Scene	VGGT (3DGS)			COLMAP (3DGS)			VGGT (GS-W)			COLMAP (GS-W)			VGGT (WeatherGS)			COLMAP (WeatherGS)		
	PSNR \uparrow	SSIM \uparrow	LPIPS \downarrow	PSNR \uparrow	SSIM \uparrow	LPIPS \downarrow	PSNR \uparrow	SSIM \uparrow	LPIPS \downarrow	PSNR \uparrow	SSIM \uparrow	LPIPS \downarrow	PSNR \uparrow	SSIM \uparrow	LPIPS \downarrow	PSNR \uparrow	SSIM \uparrow	LPIPS \downarrow
corner	17.458	0.453	0.453	\times	\times	\times	19.253	0.561	0.387	\times	\times	\times	17.282	0.392	0.413	\times	\times	\times
beartoy	17.249	0.625	0.435	21.452	0.785	0.343	19.474	0.711	0.415	18.623	0.688	0.451	15.611	0.584	0.442	19.993	0.723	0.332
bicycle	19.670	0.456	0.353	20.822	0.647	0.253	19.722	0.496	0.361	17.864	0.443	0.559	19.278	0.404	0.328	20.227	0.512	0.280
dustbin	16.780	0.374	0.568	19.414	0.516	0.431	19.205	0.484	0.691	\times	\times	\times	17.069	0.347	0.467	\times	\times	\times
flower	14.272	0.188	0.578	16.649	0.336	0.464	14.814	0.283	0.667	\times	\times	\times	9.977	0.098	0.723	10.710	0.118	0.726
parkbear	17.479	0.435	0.464	\times	\times	\times	18.953	0.507	0.490	\times	\times	\times	17.271	0.376	0.441	\times	\times	\times
popmart	17.404	0.631	0.506	16.376	0.665	0.473	17.632	0.714	0.500	15.776	0.680	0.608	15.995	0.582	0.496	15.202	0.598	0.459
rustydesk	21.255	0.484	0.429	21.741	0.615	0.377	21.498	0.543	0.499	17.813	0.500	0.704	20.721	0.419	0.365	21.726	0.539	0.322
stone	20.538	0.552	0.402	20.128	0.659	0.349	21.688	0.603	0.439	21.620	0.627	0.489	21.043	0.564	0.307	19.990	0.586	0.334
door	16.957	0.582	0.406	\times	\times	\times	18.986	0.650	0.431	\times	\times	\times	16.997	0.519	0.380	\times	\times	\times

Table 5. Comparison of camera pose estimation (AUC@30 [33]) and the number of points in the point cloud between VGGT and COLMAP on background- and raindrop-focused datasets. BG-focused = background-focused, RD-focused = raindrop-focused.

	VGGT		COLMAP	
	BG-focused	RD-focused	BG-focused	RD-focused
AUC@30	0.91	0.34	0.79	0.17
Num. of Points	69401.11	x	5476.89	302.50

drops. Uformer and Restormer outperform WeatherGS in restoring raindrop-degraded images. Among 3DGS variants, 3DGS suffers from detail loss, GS-W introduces artifacts, and 3DGS-MCMC offers improved quality over 3DGS. Weather-GS exhibits considerable blurriness due to limitations in handling raindrop-degraded images but shows strong multi-view consistency.

In scenes that both COLMAP and VGGT successfully reconstruct, COLMAP recovers finer geometric and photometric detail. However, under raindrop interference, COLMAP fails to reconstruct any raindrop-focused scenes from its estimated camera poses and point clouds. By contrast, VGGT demonstrates superior robustness.

4.4. Discussion

Our benchmark reveals how raindrop-induced degradations affect the entire 3DGS reconstruction pipeline. We summarize three key insights as follows.

Impact of Different Focus Conditions As shown in Table 5, raindrop-affected images significantly degrade the accuracy of camera pose estimation and point cloud initialization, especially under raindrop-focused conditions. Although VGGT provides improved robustness on background-focused images, it still fails easily when strong blur and focal-plane shifts occur in raindrop-focused views. These observations suggest that future methods must ex-

plicitly handle the geometric ambiguities introduced by focus shifts and adherent raindrops. Moreover, downstream 3D reconstruction should incorporate strategies that can tolerate inaccurate poses and sparse or noisy point clouds, as these errors propagate throughout the entire 3DGS optimization process.

Impact of Raindrop Removal Methods Table 2 shows that applying robust raindrop removal methods can improve 3D reconstruction quality. However, a substantial performance gap remains, indicating that raindrop removal alone is insufficient for reliable reconstruction. In practice, downstream 3DGS methods must remain effective even when the removal results are imperfect, making it necessary to leverage multi-view information to compensate for incomplete or inaccurate restoration. Moreover, the removal quality varies across views, introducing multi-view inconsistencies that propagate into 3DGS optimization and often manifest as floaters or structural artifacts. Addressing these inconsistencies and improving robustness to imperfect raindrop removal will be important directions for future research.

Impact of 3DGS Methods Table 2 indicates the performance of various 3DGS approaches under raindrop-affected scenes. Overall, GS-W [43] achieves the best reconstruction quality, largely due to its robustness to inconsistent or transient objects. In our setting, raindrops naturally behave as view-inconsistent elements, and GS-W’s design allows it to better tolerate such variability. This observation suggests that future research should explore reconstruction strategies that explicitly account for view inconsistency, transient artifacts, or incomplete observations, enabling 3DGS pipelines to remain stable even under severe multi-view degradations.

5. Conclusion

In summary, RaindropGS offers a novel benchmark for evaluating 3DGS methods under real-world raindrop conditions. By addressing the limitations of previous synthetic

datasets, we provide a more effective assessment of 3DGS performance in practical, unconstrained environments. Through the evaluation of multiple 3DGS variants, we identify the accumulated errors in camera pose estimation, point cloud initialization, raindrop removal, and 3DGS methods. Our findings highlight the strengths and weaknesses of existing approaches, offering insights into their performance under raindrop-corrupted conditions. These results underscore the need for more robust techniques to handle diverse raindrop characteristics and multi-view inconsistencies. RaindropGS not only contributes to the advancement of 3D reconstruction under challenging conditions but also lays the foundation for future research aimed at improving 3DGS performance in real-world applications.

References

- [1] Yanqi Bao, Tianyu Ding, Jing Huo, Yaoli Liu, Yuxin Li, Wenbin Li, Yang Gao, and Jiebo Luo. 3d gaussian splatting: Survey, technologies, challenges, and opportunities. *IEEE Transactions on Circuits and Systems for Video Technology*, 2025. 3
- [2] Max Born and Emil Wolf. *Principles of optics: electromagnetic theory of propagation, interference and diffraction of light*. Elsevier, 2013. 4
- [3] Wenhui Chang, Hongming Chen, Xin He, Xiang Chen, and Liangduo Shen. Uav-rain1k: A benchmark for raindrop removal from uav aerial imagery. In *Proceedings of the IEEE/CVF Conference on Computer Vision and Pattern Recognition*, pages 15–22, 2024. 1
- [4] Qiyu Dai, Xingyu Ni, Qianfan Shen, Wenzheng Chen, Baoquan Chen, and Mengyu Chu. Rainygs: Efficient rain synthesis with physically-based gaussian splatting. In *Proceedings of the Computer Vision and Pattern Recognition Conference*, pages 16153–16162, 2025. 1
- [5] Yang Fu, Sifei Liu, Amey Kulkarni, Jan Kautz, Alexei A Efros, and Xiaolong Wang. Colmap-free 3d gaussian splatting. In *Proceedings of the IEEE/CVF Conference on Computer Vision and Pattern Recognition*, pages 20796–20805, 2024. 1
- [6] Yasutaka Furukawa, Carlos Hernández, et al. Multi-view stereo: A tutorial. *Foundations and trends® in Computer Graphics and Vision*, 9(1-2):1–148, 2015. 5
- [7] Zhixiang Hao, Shaodi You, Yu Li, Kunming Li, and Feng Lu. Learning from synthetic photorealistic raindrop for single image raindrop removal. In *Proceedings of the IEEE/CVF International Conference on Computer Vision Workshops*, pages 0–0, 2019. 4
- [8] Richard Hartley and Andrew Zisserman. *Multiple view geometry in computer vision*. Cambridge university press, 2003. 4
- [9] Zhisheng Huang, Peng Wang, Jingdong Zhang, Yuan Liu, Xin Li, and Wenping Wang. 3r-gs: Best practice in optimizing camera poses along with 3dgs. *arXiv preprint arXiv:2504.04294*, 2025. 1
- [10] Yeying Jin, Xin Li, Jiadong Wang, Yan Zhang, and Malu Zhang. Raindrop clarity: A dual-focused dataset for day and night raindrop removal. In *European Conference on Computer Vision*, pages 1–17. Springer, 2024. 4, 5
- [11] Bernhard Kerbl, Georgios Kopanas, Thomas Leimkühler, and George Drettakis. 3d gaussian splatting for real-time radiance field rendering. *ACM Trans. Graph.*, 42(4):139–1, 2023. 2, 5, 7, 8
- [12] Shakiba Kheradmand, Daniel Rebain, Gopal Sharma, Weiwei Sun, Yang-Che Tseng, Hossam Isack, Abhishek Kar, Andrea Tagliasacchi, and Kwang Moo Yi. 3d gaussian splatting as markov chain monte carlo. *Advances in Neural Information Processing Systems*, 37:80965–80986, 2024. 2, 5, 7
- [13] Dmytro Kotovenko, Olga Grebenkova, and Björn Ommer. Edgs: Eliminating densification for efficient convergence of 3dgs. *arXiv preprint arXiv:2504.13204*, 2025. 1
- [14] Jonas Kulhanek, Songyou Peng, Zuzana Kukelova, Marc Pollefeys, and Torsten Sattler. Wildgaussians: 3d gaussian splatting in the wild. *arXiv preprint arXiv:2407.08447*, 2024. 3
- [15] Xin Li, Yeying Jin, Xin Jin, Zongwei Wu, Bingchen Li, Yufei Wang, Wenhan Yang, Yu Li, Zhibo Chen, Bihai Wen, et al. Ntire 2025 challenge on day and night raindrop removal for dual-focused images: Methods and results. In *Proceedings of the Computer Vision and Pattern Recognition Conference*, pages 1172–1183, 2025. 1
- [16] Yizhou Li, Yusuke Monno, and Masatoshi Okutomi. Dual-pixel raindrop removal. *IEEE Transactions on Pattern Analysis and Machine Intelligence*, 2024. 1
- [17] Yunhao Li, Jing Wu, Lingzhe Zhao, and Peidong Liu. Derrainnerf: 3d scene estimation with adhesive waterdrop removal. In *2024 IEEE International Conference on Robotics and Automation (ICRA)*, pages 2787–2793. IEEE, 2024. 1, 3, 4
- [18] Shuhong Liu, Xiang Chen, Hongming Chen, Quanfeng Xu, and Mingrui Li. Deraings: Gaussian splatting for enhanced scene reconstruction in rainy environments. In *Proceedings of the AAAI Conference on Artificial Intelligence*, pages 5558–5566, 2025. 1, 3, 4
- [19] Xianqiang Lyu, Hui Liu, and Junhui Hou. Rainyscape: Unsupervised rainy scene reconstruction using decoupled neural rendering. In *Proceedings of the 32nd ACM International Conference on Multimedia*, pages 10920–10929, 2024. 1
- [20] Ben Mildenhall, Pratul P Srinivasan, Matthew Tancik, Jonathan T Barron, Ravi Ramamoorthi, and Ren Ng. Nerf: Representing scenes as neural radiance fields for view synthesis. *Communications of the ACM*, 65(1):99–106, 2021. 3
- [21] Zhongyan Niu, Zhen Tan, Jinpu Zhang, Xueliang Yang, and Dewen Hu. Hgsloc: 3dgs-based heuristic camera pose refinement. In *2025 IEEE International Conference on Robotics and Automation (ICRA)*, pages 1–7. IEEE, 2025. 1
- [22] Maxime Oquab, Timothée Darcret, Théo Moutakanni, Huy Vo, Marc Szafraniec, Vasil Khalidov, Pierre Fernandez, Daniel Haziza, Francisco Massa, Alaaeldin El-Nouby, et al. Dinov2: Learning robust visual features without supervision. *arXiv preprint arXiv:2304.07193*, 2023. 5
- [23] Weihong Pan, Xiaoyu Zhang, Hongjia Zhai, Xiaojun Xiang, Hanqing Jiang, and Guofeng Zhang. Liberated-gs: 3d

gaussian splatting independent from sfm point clouds. In *Proceedings of the IEEE/CVF International Conference on Computer Vision*, pages 26675–26685, 2025. 1

[24] William Peebles and Saining Xie. Scalable diffusion models with transformers. In *Proceedings of the IEEE/CVF international conference on computer vision*, pages 4195–4205, 2023. 3

[25] Ivana Petrovska and Boris Jutzi. Impact of rain on 3d reconstruction with multi-view stereo, neural radiance fields and gaussian splatting. *ISPRS Annals of the Photogrammetry, Remote Sensing and Spatial Information Sciences*, 10:169–176, 2025. 1

[26] Ivana Petrovska and Boris Jutzi. Seeing beyond vegetation: A comparative occlusion analysis between multi-view stereo, neural radiance fields and gaussian splatting for 3d reconstruction. *ISPRS Open Journal of Photogrammetry and Remote Sensing*, page 100089, 2025. 1

[27] Chenghao Qian, Yuhu Guo, Wenjing Li, and Gustav Markkula. Weathergs: 3d scene reconstruction in adverse weather conditions via gaussian splatting. *arXiv preprint arXiv:2412.18862*, 2024. 1, 2, 3, 4, 5, 7, 8

[28] Rui Qian, Robby T Tan, Wenhan Yang, Jiajun Su, and Jiaying Liu. Attentive generative adversarial network for raindrop removal from a single image. In *Proceedings of the IEEE conference on computer vision and pattern recognition*, pages 2482–2491, 2018. 2, 3, 5, 6

[29] Rui Qian, Robby T Tan, Wenhan Yang, Jiajun Su, and Jiaying Liu. Attentive generative adversarial network for raindrop removal from a single image. In *Proceedings of the IEEE conference on computer vision and pattern recognition*, pages 2482–2491, 2018. 3

[30] Johannes L Schonberger and Jan-Michael Frahm. Structure-from-motion revisited. In *Proceedings of the IEEE conference on computer vision and pattern recognition*, pages 4104–4113, 2016. 5

[31] Johannes L Schonberger and Jan-Michael Frahm. Structure-from-motion revisited. In *Proceedings of the IEEE conference on computer vision and pattern recognition*, pages 4104–4113, 2016. 2, 5, 6, 8

[32] Ming-Wen Shao, Le Li, De-Yu Meng, and Wang-Meng Zuo. Uncertainty guided multi-scale attention network for raindrop removal from a single image. *IEEE Transactions on Image Processing*, 30:4828–4839, 2021. 3

[33] Jianyuan Wang, Christian Rupprecht, and David Novotny. Posediffusion: Solving pose estimation via diffusion-aided bundle adjustment. In *Proceedings of the IEEE/CVF International Conference on Computer Vision*, pages 9773–9783, 2023. 8

[34] Jiaxu Wang, Ziyi Zhang, Junhao He, and Renjing Xu. Pfgs: High fidelity point cloud rendering via feature splatting. In *European Conference on Computer Vision*, pages 193–209. Springer, 2024. 1

[35] Jianyuan Wang, Minghao Chen, Nikita Karaev, Andrea Vedaldi, Christian Rupprecht, and David Novotny. Vggt: Visual geometry grounded transformer. In *Proceedings of the Computer Vision and Pattern Recognition Conference*, pages 5294–5306, 2025. 2, 5, 6, 7, 8

[36] Weijia Wang. Real-time fast 3d reconstruction of heritage buildings based on 3d gaussian splashing. In *2024 IEEE 2nd International Conference on Sensors, Electronics and Computer Engineering (ICSECE)*, pages 1014–1018. IEEE, 2024. 1

[37] Zhendong Wang, Xiaodong Cun, Jianmin Bao, Wengang Zhou, Jianzhuang Liu, and Houqiang Li. Uformer: A general u-shaped transformer for image restoration. In *Proceedings of the IEEE/CVF conference on computer vision and pattern recognition*, pages 17683–17693, 2022. 2, 3, 5, 6, 7

[38] Jie Xiao, Xueyang Fu, Aiping Liu, Feng Wu, and Zheng-Jun Zha. Image de-raining transformer. *IEEE transactions on pattern analysis and machine intelligence*, 45(11):12978–12995, 2022. 2, 3, 5, 6, 7

[39] Shaodi You, Robby T Tan, Rei Kawakami, and Katsushi Ikeuchi. Adherent raindrop detection and removal in video. In *Proceedings of the IEEE Conference on Computer Vision and Pattern Recognition*, pages 1035–1042, 2013. 1

[40] Shaodi You, Robby T Tan, Rei Kawakami, Yasuhiro Mukaigawa, and Katsushi Ikeuchi. Adherent raindrop modeling, detection and removal in video. *IEEE transactions on pattern analysis and machine intelligence*, 38(9):1721–1733, 2015. 1

[41] Zehao Yu, Anpei Chen, Binbin Huang, Torsten Sattler, and Andreas Geiger. Mip-splatting: Alias-free 3d gaussian splatting. In *Proceedings of the IEEE/CVF conference on computer vision and pattern recognition*, pages 19447–19456, 2024. 1

[42] Syed Waqas Zamir, Aditya Arora, Salman Khan, Munawar Hayat, Fahad Shahbaz Khan, and Ming-Hsuan Yang. Restormer: Efficient transformer for high-resolution image restoration. In *Proceedings of the IEEE/CVF conference on computer vision and pattern recognition*, pages 5728–5739, 2022. 2, 3, 5, 6, 7

[43] Dongbin Zhang, Chuming Wang, Weitao Wang, Peihao Li, Minghan Qin, and Haoqian Wang. Gaussian in the wild: 3d gaussian splatting for unconstrained image collections. In *European Conference on Computer Vision*, pages 341–359. Springer, 2024. 1, 2, 5, 7, 8

[44] Chengxuan Zhu, Renjie Wan, Yunkai Tang, and Boxin Shi. Occlusion-free scene recovery via neural radiance fields. In *Proceedings of the IEEE/CVF Conference on Computer Vision and Pattern Recognition*, pages 20722–20731, 2023. 1